Tribology International 44 (2011) 180–186

Contents lists available at ScienceDirect

Tribology International

journal homepage: www.elsevier.com/locate/triboint

Frictional performance of silica microspheres

Steven G. Vilt, Nathaniel Martin, Clare McCabe, G. Kane Jennings *

Department of Chemical and Biomolecular Engineering, Vanderbilt University, VU Station B 351604, Nashville, TN 37235-1604, USA

ARTICLE INFO

Article history:
Received 11 August 2010
Received in revised form
20 October 2010
Accepted 25 October 2010
Available online 31 October 2010

Keywords:
Rolling element
Micro-/nano-scale friction
Ball bearings
Friction

ABSTRACT

We present a fundamental study of the frictional performance of silica microspheres, either 4, 2, or 0.5 μm in diameter, on a silicon substrate. The tribological properties of these rolling systems were measured with a ball-on-flat tribometer at various loads. The frictional performance of the rolling systems is found to be highly dependent on load and sphere diameter. Rolling motion was confirmed by imaging the surface of microsphere systems that have been coated with a thin layer of gold. In addition, the surface energy of the lubrication scheme was altered using coatings containing octadecyltrichlorosilane or (tridecafluoro-1,1,2,2-tetrahydrooctyl)-1-trichlorosilane precursors.

1. Introduction

Introducing a rolling element between two contacting surfaces can greatly reduce friction, as rolling can produce frictional forces that are 10^2–10^3 times lower than those due to sliding [1]. Despite the well-known frictional benefits of rolling motion, few experimental investigations of rolling friction have been performed on the micro and nanoscale [1–8]. In contrast to macroscopic studies where adhesion is relatively unimportant and rolling friction dominates, interfacial interactions grow in importance as the dimensions of the rolling element shrink to the microscale and below, and friction can be composed of both rolling and sliding [9,10]. Furthermore, the pressure and contact areas inherent in a microscale system are different than those seen on the macroscale [11].

Prior investigations of rolling friction have focused on rolling elements larger than 40 μm [2,5–8,12] and those of molecular dimensions [1,3,4,13–15]. Beerschwinger et al. [5] reported coefficient of friction values of 0.05 for 40 μm diameter glass spheres rolling between two flat surfaces and Waits et al. [6] reported a 0.01 value for a tribological system containing 285 μm diameter stainless steel ball bearings. More recently, Sinha et al. [8] reported coefficients of friction as low as 0.005 for 53 μm glass microspheres contained between two rotating silicon plates. At the nanoscale, experimental investigations of rolling friction have focused on hollow nanoparticles such as C_{60} fullerenes [3] or fullerene-like supramolecules consisting of WS_2 or MoS_2 [4]. While all these studies have demonstrated the advantages of rolling over sliding in reducing frictional forces and wear, a key size range (200 nm–5 μm) between these extremes that is compatible with MEMS and modern micro-fabrication technologies has not been explored.

In this work, we present a simple lubrication scheme based on a layer of silica spheres that are deposited onto a flat silicon substrate. To investigate the effect of sphere size and load on frictional performance, the diameters of the spheres were varied (4, 2, or 0.5 μm), and testing was done at multiple loads with a ball-on-flat microtribometer. A 10–50 μm contact radius exists between the sample and the spherical probe tips used during testing, creating microscale contact areas similar to those which would be found in MEMS devices [16]. The goal of the work was to assess whether low friction rolling could be established at this size scale and to identify critical parameters, such as the surface coverage of the spheres, which must be satisfied for effective lubrication. Sphere confinement suitable for extended cyclic testing, which has been achieved at larger dimensions [6], is outside the scope of the present work. To confirm that rolling friction is being achieved, a simple test based on the deposition of a thin gold coating onto the microsphere system was developed and introduced. We show that the coefficient of friction and wear life of the lubrication system are dependent on both sphere diameter and load, as the individual spheres must withstand the contact pressures applied during testing.

In addition, the silica spheres and silicon substrate can be modified by the addition of monolayer films to investigate the effect of surface composition on microscale rolling friction. Molecularly thin films can be formed on the spheres and surrounding surfaces with trichlorosilane precursors, as the trichlorosilane moieties covalently bind to the spheres and substrate through siloxane linkages [17–19]. Previous studies investigating sliding friction on silicon substrates found that trichlorosilane monolayers

* Corresponding author. Tel.: +1 615 322 2707; fax: +1 615 343 7951.
E-mail address: kane.g.jennings@vanderbilt.edu (G. Kane Jennings).

0301-679X/$ - see front matter © 2010 Elsevier Ltd. All rights reserved.
doi:10.1016/j.triboint.2010.10.024

decrease friction forces by an order of magnitude [17] and significantly reduce stiction [19,20], which is caused by capillary condensation of atmospheric water vapor [19] and can increase the coefficient of friction in rolling devices [21,22]. In the hope of improving the frictional performance of the sphere systems, we have developed a protocol to functionalize the sphere/substrate systems with molecular coatings of either octadecyltrichlorosilane (H18) or (tridecafluoro-1,1,2,2-tetrahydrooctyl)-1-trichlorosilane (F6H2) precursors. While there have been numerous studies that spray coat ball bearings [23–25], our work represents the first report of the molecular functionalization of a rolling friction system.

2. Experimental

2.1. Materials

Octadecyltrichlorosilane (H18) and (tridecafluoro-1,1,2,2-tetrahydrooctyl)-1-trichlorosilane (F6H2) were purchased from United Chemical Technologies. 30% hydrogen peroxide (H_2O_2), methylene chloride, and toluene were purchased from Fisher Scientific. Sulfuric acid (H_2SO_4) was purchased from EMD Chemicals, Inc. All reagents and chemicals were used as received. Silicon (1 0 0) wafers were obtained from Wafer Reclaim Services, LLC. 10 mL of a water solution containing a 5% mass fraction of silicon oxide spheres, with diameters of 4, 2, or 0.5 μm, were obtained from Corpuscular Inc. The coefficients of variation for the spheres were $<2\%$ for the 4 and 2 μm spheres and $<3\%$ for the 0.5 μm spheres.

2.2. Preparation of silicon substrates

Silicon wafers were first cut into $4 \times 1.3\ cm^2$ pieces using a diamond-tip stylus. The silicon samples were sequentially rinsed with ethanol, water, and again with ethanol, dried in a stream of N_2, and then sonicated in ethanol for 30 min to displace any remaining contaminants. After sonication, the samples were rinsed sequentially with water and ethanol, dried in a stream of N_2, and placed in piranha solution (14 mL H_2SO_4:6 mL H_2O_2) for 30 min to hydroxylate the silicon oxide surface. The piranha-treated substrates were rinsed 3 times by submersion in water. All samples were rinsed once more with a stream of DI water, briefly rinsed with ethanol, and thoroughly dried with N_2 before the silicon oxide spheres were deposited on the surface.

2.3. Deposition of silicon oxide spheres

400 μL of a well-mixed aqueous solution containing a 0.08% sphere mass fraction was deposited on the silicon substrates with a pipette. The samples were then placed in a vacuum chamber and put under a reduced pressure of 0.03 Torr for 10 min. The 10 min time period was found to be adequate to allow the spheres suspended in the solution to adhere to the substrate surface, but is sufficiently brief to prevent bubble defects from forming. The samples were then removed from the chamber and the excess water on the substrates was siphoned off the surface with a micropipette. The samples were then once again placed under reduced pressure for 10 min to evaporate any remaining water. Finally, all samples were sequentially rinsed with a gentle stream of ethanol and water, and then thoroughly dried with N_2 (the particles remain adhered to the surface throughout the rinsing and drying process). The samples were stored in Petri dishes until testing or functionalization was performed.

2.4. Monolayer coatings of sphere systems

The trichlorosilane monolayers were formed by immersing the substrates, which were already layered with 2 μm diameter silicon oxide spheres, into 1 mM solutions of either the H18 or F6H2 precursors. The solution solvent was 20 mL of either toluene (H18) or methylene chloride (F6H2). The F6H2 samples were removed from the F6H2/methylene chloride solution after 20 min, sequentially rinsed with methylene chloride, ethanol, water, and again with ethanol, and dried in a stream of N_2. The H18 samples were removed from the H18/toluene solution after 5 h, sequentially rinsed with toluene, ethanol, water, and again with ethanol, and dried in a stream of N_2. The samples were stored in Petri dishes until characterization or testing was performed.

2.5. Optical microscopy

Microscope images of the samples were acquired using an Olympus BX41 microscope with Pixera camera and Pixera Viewfinder Pro software. Two magnification lens were used (10*x* and 25*x*) to produce the images. Quantitative analysis of coverage area was achieved by using Image J software. The color contrast within the optical images was maximized and the sphere coverage was determined using the contrast distribution analysis tool. The coverage areas were determined by averaging the results of at least 3 separate images. The reported values and errors reflect the average and standard deviation of at least 4 independently prepared samples.

2.6. Scanning electron microscope

Scanning electron images were obtained using a Raith e-Line electron beam lithography (EBL) system equipped with a thermal-assisted field emission gun at 10 keV.

2.7. Contact angle

Contact angles of water were measured with a Rame-Hart manual contact angle goinometer. Advancing and receding contact angles were obtained on both sides of approximately 10 μL drops with the syringe in the probe droplet during measurements. The reported values and errors reflect the average and standard deviation of at least 4 independently prepared samples.

2.8. Micro-scale friction testing

Micro-scale friction tests were performed in open air with a ball-on-flat micro-tribotester (Center for Tribology, Inc.) using two separate sensors, a 2-D FVL force sensor and a DFM-0.5 force sensor. The FVL sensor is capable of measuring forces from 1 to 100 mN in both dimensions and was used to perform cyclic friction tests with a constant load of 9.8 mN. The probe tip was a 1 mm diameter stainless steel ball firmly glued onto the end of an 8 mm long pin and attached to the sensor via a suspension mounting cantilever. The DFM sensor can apply loads from 50 to 50,000 mN and was used to perform cyclic friction tests with a constant load of 98, 245, 490, and 980 mN. For these higher loads, the probe tip was a 4 mm diameter stainless steel ball contained in a holder. The arithmetical mean roughness (R_a) of the 4 mm balls was determined using an Olympus laser confocal microscope and was found to be 13 ± 3 nm. The contact radii achieved during testing was estimated using SEM images of the probe paths and found to be between 10 and 50 μm. All tests were conducted with a sliding speed of 1 mm/s and a scan length of 10 mm. Unless specified, the frictional tests were terminated once the coefficient of friction reached 0.20. Three

tests were performed for each load on each sample. The coefficient of friction (μ) was determined using Amonton's law, $F_f = \mu F_n$, where the friction force (F_f) is proportional to the normal force load (F_n). The reported coefficients of friction (μ) were determined by averaging the forces measured during the low-friction rolling stage. The reported values and errors reflect the averages and standard deviations of at least 4 independently prepared samples.

3. Results and discussion

3.1. Sphere dispersion and confirmation of rolling

To create the submonolayer coatings of silica spheres, a sphere/water solution was pipetted onto the silicon substrates, and then, the entire sample was placed under a reduced pressure. To prevent bubble defects from forming, the samples were returned to atmospheric pressure after 10 min and any remaining water on the surface was mechanically drawn off. The samples were then once again placed under vacuum to evaporate any remaining water. Using optical images, the coverage area for the three sphere sizes were estimated to be $56 \pm 8\%$ (4 μm dia.), $51 \pm 5\%$ (2 μm dia.), and $46 \pm 4\%$ (0.5 μm dia.), whereas perfect 2-D hexagonal sphere packing would result in 90% coverage. Attempts to increase the surface coverage above the reported values, by increasing the sphere concentration or volume of the solution, resulted in multilayering and vertical aggregates.

During the evaporation process, the silica spheres aggregate due to adhesive interactions between the silica spheres while in the water solution [26]. These microscale clusters are shown in the SEM images presented in Fig. 1(a–c). The attractive forces between the spheres become more significant with decreasing diameter [27] and, therefore, clustering is more pronounced for the smallest sphere size (Fig. 1(c)). During frictional testing, the rolling motion of the spheres disrupts the adhesive interactions, and the aggregates disperse to create a more microscopically uniform coverage (Fig. 2(a)). To confirm that rolling motion is occurring during frictional testing, we sputtered a ~10 nm thick coating of gold onto a 2 μm microsphere system. The coated samples were then tested with the tribometer and imaged with a scanning electron microscope. Since the underside of the spheres will not be exposed during sputtering, janus (or "two-faced") spheres are created which contain a gold-coated region and a relatively bare silica region, which will become visible as the janus spheres roll during frictional testing. SEM imaging shows the bare silica regions of the spheres (Fig. 1(d)), which confirms that rolling motion does occur. Furthermore, the weakly-adhered gold coating on the sphere was occasionally worn away upon probe-sphere contact. Fig. 1(d) clearly shows wear patterns which extend around the circumferences of the spheres, providing additional support that the sphere is rolling as it contacts the probe.

3.2. Frictional performance of rolling-element lubrication systems

Fig. 2 shows a typical frictional test at a load of 98 mN for the 2 μm sphere system. An immediate decrease in friction is observed for the first few cycles, followed by an extended period of low friction, and then, an eventual rapid increase in the coefficient of friction. We believe that the higher frictional forces observed during the first few passes are due to the collisions occurring between the closely packed sphere clusters. To investigate the effect of close packing, microsphere systems that have lower initial

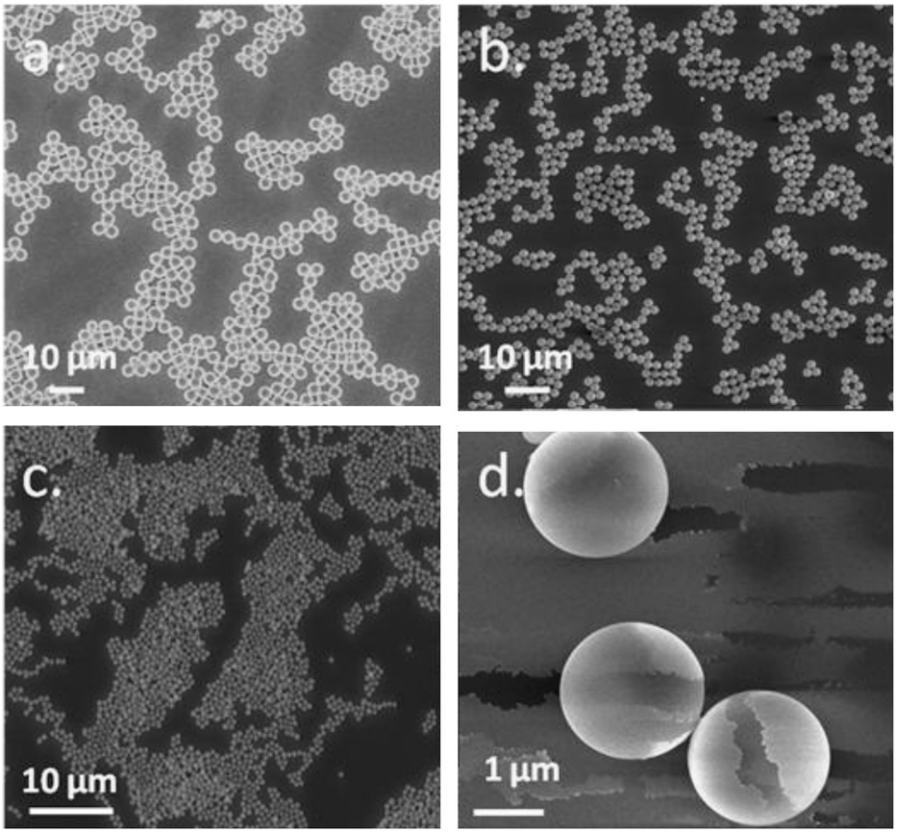

Fig. 1. SEM images of the microsphere systems studied. Images (a)–(c) show the dispersion of the 4 μm diameter (a), 2 μm diameter (b), and 0.5 μm diameter (c) microsphere systems before frictional testing was performed. Image (d) displays the exposure of the uncoated "bottom" and the circumferential wear-tracks of the 2 μm spheres coated with 10 nm of gold, which demonstrates that rolling friction is being achieved.

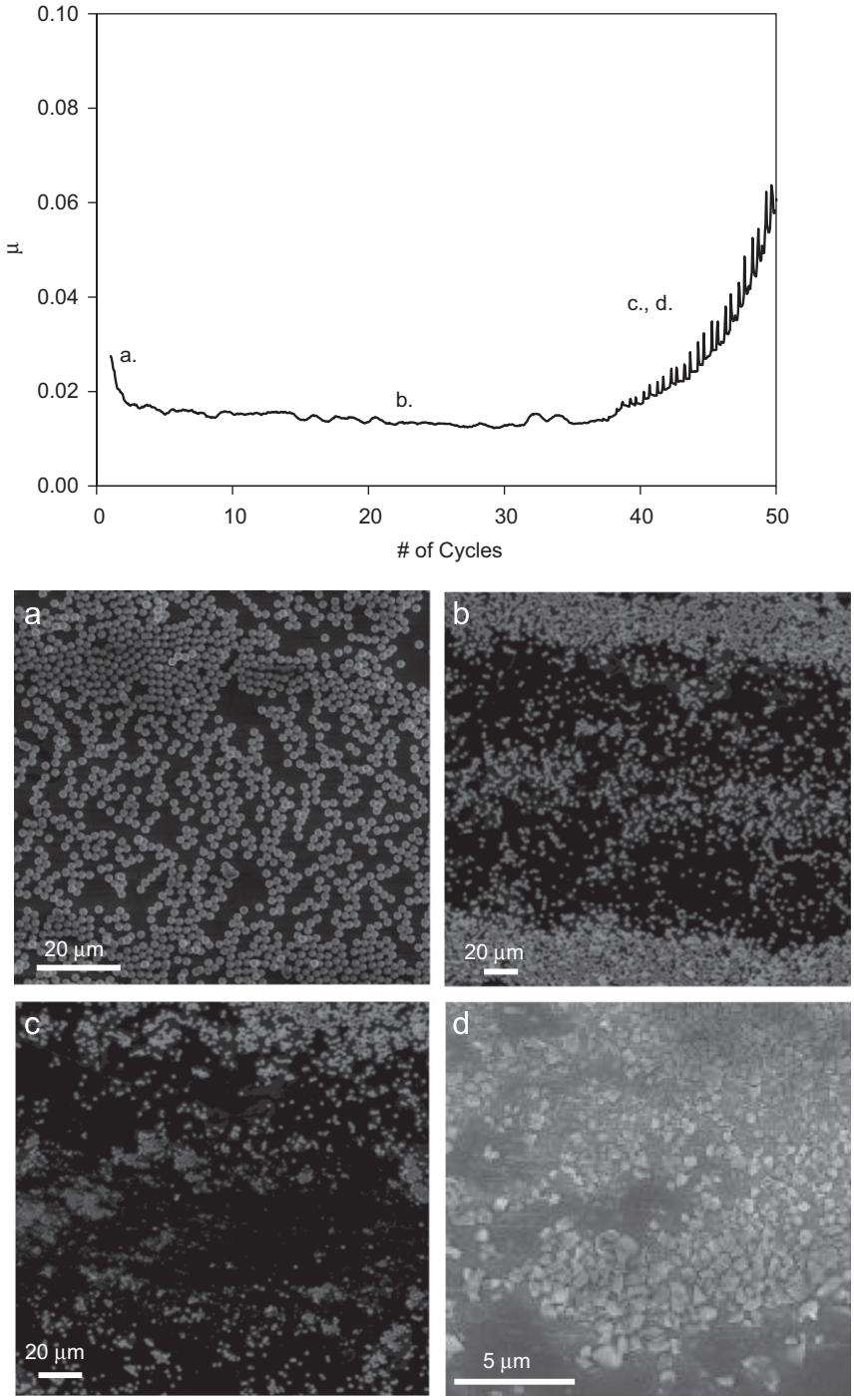

Fig. 2. (top) Long-term frictional performance of the 2 μm diameter sphere system. The cyclic tribology test was performed with a 4 mm diameter stainless steel ball contained in a holder at 1.0 mm/s with a scan length of 10 mm. (bottom) SEM images of the 2 μm diameter sphere system show areal coverage during different stages of the cyclic test. Once the sphere coverage decreases to a critical level the pressure of the probe causes fragmentation of the individual sphere elements (d).

surface coverages ($34 \pm 4\%$) than the reported averages were tested. These sparser systems did not exhibit the initial high friction forces, which supports our claim that the collisions between the spheres resists the initial rolling motion [13] and results in slightly higher friction. After a few passes the dispersion of the spheres (Fig. 2(b)) allows unhindered rolling to be established. The substrate is devoid of any confinement barriers and, therefore, the wear track continually widens during testing as the spheres become more dispersed (Fig. 2(a and b)). Once the surface coverage decreases below a critical threshold (discussed further below), the pressure on the individual spheres becomes too great; instead of rolling, spheres begin to experience excessive compression and fracture (Fig. 2(c and d)), which increases the coefficient of friction. As testing continues, the remaining intact spheres experience even greater stress and eventually all the silica spheres are either crushed or dispersed, resulting in probe-substrate contact and a dramatic increase in the coefficient of friction. Complete failure occurs once the sphere fragments are pushed towards the ends of the wear track (Fig. S1, Supplementary information). At this phase the probe is scratching the silicon substrate, and the

coefficient of friction values increase to ~0.6, which corresponds to the values achieved for a bare silicon substrate.

To investigate the influence of load and sphere diameter on microscale rolling friction, we tested the three sphere systems at five loads: 9.8, 98, 245, 490, and 980 mN. The reported coefficients of friction (μ) were determined by averaging the forces measured during the low-friction rolling stage. As shown in Fig. 3, the frictional performance is dependent on load and sphere diameter. The 0.5 μm system, which will be discussed further below, only achieved rolling friction at the lowest load tested, while rolling friction was established up to 980 mN for the 4 and 2 μm systems. At the 9.8, 98, and 245 mN loads, the 4 and 2 μm sphere systems produced test profiles very similar to Fig. 2 and achieved extremely low coefficients of friction that were statistically indistinguishable from each other. Specifically, the 4 μm system had coefficient of friction values of 0.021 ± 0.006 (9.8 mN), 0.021 ± 0.004 (98 mN), and 0.020 ± 0.005 (245 mN), while the 2 μm system had coefficient of friction values of $0.020 \pm .004$ (9.8 mN), 0.019 ± 0.003 (98 mN), and 0.021 ± 0.004 (245 mN). The frictional benefit of rolling over sliding is considerable; the ~0.02 values achieved for the silica spheres is 30*x* less than the value achieved for tribometer testing on a flat silicon surface [17]. When the load is increased to 490 mN the coefficient of friction increases to 0.026 ± 0.005 (4 μm) and 0.035 ± 0.009 (2 μm) as the increased testing load puts a greater contact pressure on the spheres and begins to hinder the rolling motion [13,28]. At 980 mN the rolling motion is severely affected and the coefficients of friction increase significantly to 0.08 ± 0.036 (4 μm) and 0.12 ± 0.035 (2 μm).

The wear life of the sphere systems was also investigated and is presented in Fig. 4. Failure was easily identified by a sudden spike in coefficient of friction and a dramatic increase in data noise (Fig. S2, Supplementary information). The trends are similar for the 4 and 2 μm systems, as the 9.8 mN and 98 mN loads resulted in comparable cycle lives followed by a decrease in wear life with increasing loads. The 4 μm system achieved wear life values of 33 ± 2 cycles (9.8 mN), 32 ± 2 cycles (98 mN), 15 ± 8 cycles (245 mN), 4 ± 2 cycles (490 mN), and 1 ± 0 cycles (980 mN), while the 2 μm system achieved values of 28 ± 16 cycles (9.8 mN), 31 ± 11 cycles (98 mN), 10 ± 2 cycles (245 mN), 4 ± 1 cycles (490 mN), and 1 ± 0 cycles (980 mN). The lack of confinement within the microsphere systems is responsible for the failure; the continuous dispersal of the spheres away from the probe track results in increased pressures on the individual spheres which remain in contact with the probe, and eventually the contact pressure experienced by the spheres exceeds their material strength and fragmentation occurs. At higher loads the critical pressure is reached earlier and, therefore, the spheres are fragmented sooner (Fig. 4). The wear life is almost identical at 9.8 and 98 mN loads, which would appear to disagree with our analysis. However, the 9.8 mN load was applied with a 1 mm diameter probe, while the 98 mN load was applied with a 4 mm probe. If the applied pressure is estimated with a simplified sphere-on-flat Hertz equation [29,30] the 9.8 and 98 mN tests would produce similar pressures and, therefore, results in comparable cycle lives.

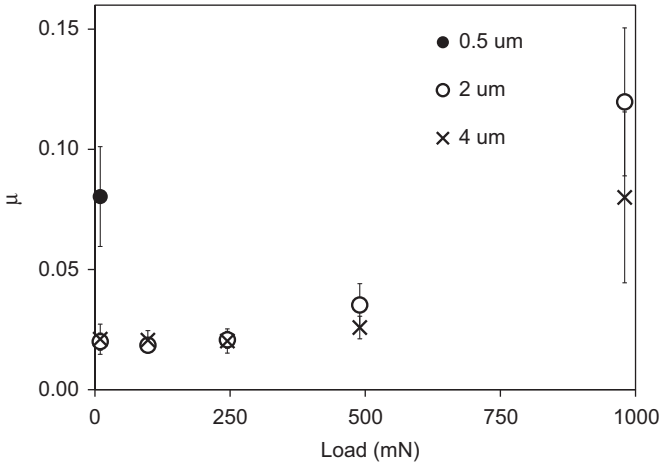

Fig. 3. Effect of sphere diameter and load on the frictional performance of the silica sphere systems studied. Cyclic tribology tests were performed with a 1 mm diameter stainless steel probe tip for the 9.8 mN loads, while all other loads used a 4 mm diameter stainless steel ball contained in a holder. Test speed was at 1.0 mm/s with a scan length of 10 mm. The coefficient of friction was determined by averaging the forces measured during the low-friction rolling stage. The 0.5 μm diameter spheres only achieved rolling friction for the 9.8 mN load, and, therefore, there is only one data point for that diameter. Reported values and error bars represent averages and standard deviations, respectively, based on at least 4 independently prepared films.

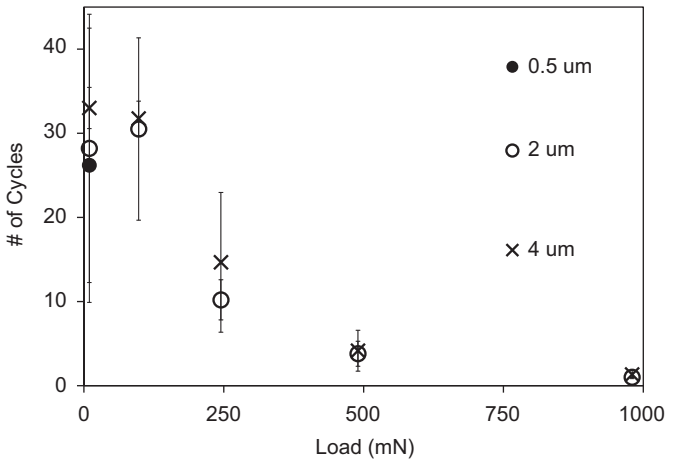

Fig. 4. Effect of sphere diameter and load on the wear life of the silica sphere systems studied. Cyclic tribology tests were performed with a 1 mm diameter stainless steel probe tip for the 9.8 mN loads, while all other loads used a 4 mm diameter stainless steel ball contained in a holder. Tests were performed at 1.0 mm/s with a scan length of 10 mm. Failure was easily identified by a sudden and drastic increase in friction and an increase in signal noise (Fig. S1). The 0.5 μm diameter spheres only achieved rolling friction for the 9.8 mN load, and, therefore, there is only one data point for that diameter. Reported values and error bars represent averages and standard deviations, respectively, based on at least 4 independently prepared samples.

The performance of the microsphere systems is dependent on sphere radius, as larger spheres result in lower coefficients of friction and longer wear lives for a given load. The size effect was only marginal between the 4 and 2 μm systems (a difference in coefficients of friction was only observed at the 490 and 980 mN loads, while the differences in cycle-life were insignificant) but was evident for the 0.5 μm spheres. While the 4 and 2 μm systems were able to achieve rolling friction up to 980 mN, the 0.5 μm spheres were able to support rolling motion only at the lowest tested load of 9.8 mN, achieving a coefficient of friction of 0.080 ± 0.02 with an average cycle-life of 26 ± 16. Even though the 98 mN load should provide a similar pressure as the 9.8 mN tests, the additional load of 98 mN was found to scatter the 500 nm spheres to a greater extent (most likely due to the increased loading rate). This additional dispersion reduced the contact area, thereby increasing the pressure above the yield strength of silica.

3.3. *Influence of surface coverage on frictional performance*

To confirm and further investigate the effect of sphere coverage on frictional performance, a series of 98 mN frictional tests with the 2 μm sphere system were performed and terminated at various times. The surface coverage of the spheres was estimated using SEM images and the coefficient of friction determined by averaging

the friction force over the last full cycle before the test was terminated. As shown in Fig. 5, a large increase in friction force occurs for the 2 μm system once the surface coverage of the spheres drops below 15%. The surface coverage was found to decrease from the initial value of 51 to 36% after only two cycles. After the first couple of passes the rate of sphere dispersion slows considerably, as it took an average of 31 cycles (Fig. 4) to reach the critical failure threshold of 15% coverage. These results support our explanation of the frictional results; the continual scattering of the spheres gradually increases the contact pressure due to decreased contact area between the spheres and the probe tip. The increased pressure hinders the motion of the spheres, increasing the coefficient of friction, and eventually, the pressure exceeds the yield strength of the spheres and the spheres crack and fragment. In addition, the identification of the minimum coverage needed offers important guidance for the development of advanced lubrication schemes that use containment of 2 μm silica ball bearings.

3.4. Monolayer functionalization of the microsphere systems

In an attempt to reduce adhesive forces and improve the performance of the microsphere system, the 2 μm sphere system was coated with monolayers consisting of H18 or F6H2 molecules. The 2 μm spheres were first deposited on the silicon substrate and then the entire surface (substrate plus spheres) was coated by immersing the sample into 1 mM solutions of the precursor molecule. The resulting coatings, which would be partially incomplete due to the inaccessible regions where there is direct sphere–substrate contact, will contain either CH_3 (H18) or CF_3 (F6H2) termini. Surface coverage, using optical images, was calculated before and after the functionalization process and was determined to be unchanged. The presence of the monolayer coating was confirmed using water contact angles. Before functionalization, the 2 μm sphere samples achieved advancing contact angles of $23 \pm 10^\circ$ and receding contact angles of $5 \pm 5^\circ$. After the CH_3 or CF_3-terminated monolayers were formed the advancing contact angles rose to $142 \pm 6^\circ$ (CH_3) and $136 \pm 12^\circ$ (CF_3), signaling a dramatic decrease in the surface energy. The high advancing contact angles achieved for the samples are greater than those reported for flat monolayers (111° for CH_3 [31,32] and 120° for CF_3 [33]) due to the surface roughness provided by the deposited spheres [34]. The surface roughness also caused high contact angle hysteresis, as the functionalized samples achieved receding contact angles of $77 \pm 5^\circ$ (CH_3) and $63 \pm 19^\circ$ (CF_3).

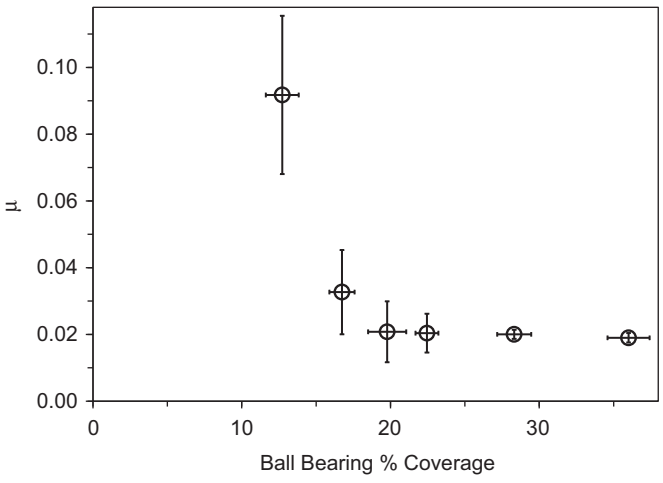

Fig. 5. Effect of sphere surface coverage on the coefficient of friction. Cyclic tribology tests, which were terminated at various times, were performed with a 4 mm diameter stainless steel ball contained in a holder with a test speed of 1.0 mm/s and a scan length of 10 mm. The areal coverage of the spheres was determined using SEM images, and the coefficient of friction was calculated by averaging the friction force over the last full cycle before the test was terminated. The entire data set was compartmentalized to produce the lowest standard deviation for sphere coverage within individual groups, with each group consisting of at least 3 data points.

The frictional performance of the functionalized samples was tested with a 98 mN load and the minimum coefficient of friction achieved for the functionalized samples was found to be similar to the unmodified samples. Specifically, the H18 monolayer samples achieved a coefficient of friction of 0.023 ± 0.0026 and the F6H2 monolayer samples resulted in a value of 0.020 ± 0.0040. The coated monolayers, however, did have significantly shorter wear lives. While the unmodified samples required 31 cycles (Fig. 4) to fail, the coated sphere systems failed in 6 ± 3 cycles (CH_3) and 12 ± 4 cycles (CF_3). The lower cycle lives of the functionalized systems suggest that the sphere coverage decreased more rapidly during testing. The low-energy surfaces achieved by functionalization would dramatically reduce the adhesive interactions between the spheres and the substrate and, thus, promote quicker dispersal of the spheres beyond the probe track. Despite the poor wear life shown by the coated samples, functionalization of the sphere/substrate system may prove beneficial in next generation lubrication schemes as shearing surfaces which confine the spheres and ball bearing systems would benefit from lower energy surfaces and easier dispersion of spheres. The monolayer coatings can greatly reduce stiction caused by liquid adhesion and capillary condensation of water vapor from the environment [19,20,35]. In addition, functionalization could be used to increase the wear life of microball bearing systems, as numerous studies at larger size scales have shown that surface coatings can delay failure [23–25,36,37].

4. Conclusion

We have investigated the frictional performance of lubrication systems based on rolling silica spheres. Silica spheres, either 4, 2, or 0.5 μm in diameter, were dispersed on silicon substrates by drop casting from an aqueous solution at reduced pressure. A simple test, involving a deposition of gold onto the microsphere system, was introduced to confirm that rolling motion has occurred. The coefficient of friction and wear life of the lubrication systems were investigated at numerous loads with a ball-on-flat microtribometer. The 4 and 2 μm systems preformed similarly, with the 4 μm spheres achieving slightly lower coefficients of friction at higher loads than the 2 μm spheres. The dependence on sphere diameter was clearly seen with the 0.5 μm system, which failed immediately at loads above 9.8 mN. The lubrication systems tested in this paper did not confine the rolling spheres and, therefore, failure was brought on by the continual dispersion of the spheres. The decrease in the surface coverage of the spheres created higher contact pressures that ultimately increased enough to fragment the individual spheres. In addition, functionalization of the sphere systems was accomplished using H18 or F6H2 precursors. The molecular coatings decreased the surface energy of the spheres and substrate, allowing the spheres to be more quickly dispersed beyond the probe track during tribometry testing. Overall, the 0.02 coefficient of friction values achieved with the 4 and 2 μm systems for numerous loads offers promise that rolling friction, if properly confined, can be utilized as a lubrication scheme for microscale devices.

Acknowledgements

This work was supported by the Office of Naval Research under Grant nos. N00014-06-1-0624, N00014-09-1-0334, and N00014-07-1-0843 and the State of Tennessee.

Appendix A. Supporting information

Supplementary data associated with this article can be found in the online version at doi:10.1016/j.triboint.2010.10.024.

References

[1] Braun OM, Tosatti E. Molecular rolling friction: the cogwheel model. J Phys: Condens Matter 2008;20(35):354007.
[2] Xiaobo T, Alireza M, Reza G. Measurement and modeling of dynamic rolling friction in linear microball bearings. J Dyn Syst-T ASME 2006;128(4):891–8.
[3] Miura K, Kamiya S, Sasaki N. C60 molecular bearings. Phys Rev Lett 2003;90(5): 055509.
[4] Rapoport L, Leshchinsky V, Lvovsky M, Nepomnyashchy O, Volovik Y, Tenne R. Mechanism of friction of fullerenes. Ind Lubr Tribol 2002;54(4):171–6.
[5] Beerschwinger U, Reuben RL, Yang SJ. Frictional study of micromotor bearings. Sens Actuators, A 1997;63(3):229–41.
[6] Waits CM, Geil B, Ghodssi R. Encapsulated ball bearings for rotary micro machines. J Micromech Microeng 2007;17(9):224–9.
[7] Ta-Wei L, Modafe A, Shapiro B, Ghodssi R. Characterization of dynamic friction in MEMS-based microball bearings. IEEE Trans Instrum Meas 2004;53(3):839–46.
[8] Sinha SK, Pang R, Tang XS. Application of micro-ball bearing on Si for high rolling life-cycle. Tribol Int 2010;43(1–2):178–87.
[9] Sitti M. Atomic force microscope probe based controlled pushing for nano-tribological characterization. IEEE ASME Trans Mechatron 2004;9(2):343–9.
[10] Chinas-Castillo F, Spikes HA. Mechanism of action of colloidal solid dispersions. J Tribol- T ASME 2003;125(3):552–7.
[11] Jiang JR, Arnell RD, Dixit G. The influence of ball size on tribological behaviour of MoS_2 coating tested on a ball-on-disk wear rig. Wear 2000;243(1–2):1–5.
[12] Ghodssi R, Denton DD, Seireg AA, Howland B. Rolling friction in a linear microactuator. 39th National Symposium of the American Vacuum Society; 1993, p. 803–7.
[13] Braun OM. Simple model of microscopic rolling friction. Phys Rev Lett 2005;95(12):126104.
[14] Li XY, Yang W. Simulating fullerene ball bearings of ultra-low friction. Nanotechnology 2007;18(11):115718.
[15] Rapoport L, Bilik Y, Feldman Y, Homyonfer M, Cohen SR, Tenne R. Hollow nanoparticles of WS2 as potential solid-state lubricants. Nature 1997;387(6635):791–3.
[16] Jack WJ. Microelectromechanical systems (MEMS): fabrication, design and applications. Smart Mater Struct 2001;10(6):1115.
[17] Vilt SG, Leng Z, Booth BD, McCabe C, Jennings GK. Surface and frictional properties of two-component alkylsilane monolayers and hydroxyl-terminated monolayers on silicon. J Phys Chem C 2009;113(33):14972–7.
[18] Srinivasan U, Houston MR, Howe RT, Maboudian R. Alkyltrichlorosilane-based self-assembled monolayer films for stiction reduction in silicon micromachines. J Microelectromech S 1998;7(2):252–60.
[19] Maboudian R, Ashurst WR, Carraro C. Self-assembled monolayers as anti-stiction coatings for MEMS: characteristics and recent developments. Sens Actuators, A 2000;82(1–3):219–23.
[20] Patton ST, Cowan WD, Eapen KC, Zabinski JS. Effect of surface chemistry on the tribological performance of a MEMS electrostatic lateral output motor. Tribol Lett 2000;9(3–4):199–209.
[21] Barquins M, Maugis D, Blouet J, Courtel R. Contact area of a ball rolling on an adhesive viscoelastic material. Wear 1978;51(2):375–84.
[22] Deryaguin BV, Karassev VV, Zakhavaeva NN, Lazarev VP. The mechanism of boundary lubrication and the properties of the lubricating film – short-range and long-range action in the theory of boundary lubrication. Prog Surf Sci 1994;45(1–4):282–95.
[23] Akdogan G, Stolarski T, Tobe S. Wear performance of polytetrafluoroethylene-metal coatings in rolling/sliding line contact. Proc IMechE Part J: J Eng. Tribol. 2003;217(2):103–14.
[24] Niebuhr D, Scholl M. Synthesis and performance of plasma-sprayed polymer/steel coating system. J Therm Spray Technol 2005;14(4):487–94.
[25] Stewart S, Ahmed R, Itsukaichi T. Rolling contact fatigue of post-treated WC-NiCrBSi thermal spray coatings. Surf Coat Tech 2005;190(2–3):171–89.
[26] Vakarelski IU, Ishimura K, Higashitani K. Adhesion between silica particle and mica surfaces in water and electrolyte solutions. J Colloid Interface Sci 2000;227(1):111–8.
[27] Yao W, Guangsheng G, Fei W, Jun W. Fluidization and agglomerate structure of SiO_2 nanoparticles. Powder Technol 2002;124(1–2):152–9.
[28] Brilliantov NV, Pöschel T. Rolling friction of a viscous sphere on a hard plane. Europhys Lett 1998;42(5):511–6.
[29] Johnson KL. Contact Mechanics. New York: Cambridge University Press; 1987.
[30] Mate MC. Tribology on the Small Scale. New York: Oxford University Press; 2008.
[31] Depalma V, Tillman N. Friction and wear of self-assembled trichlorosilane monolayer films on silicon. Langmuir 1989;5(3):868–72.
[32] Tillman N, Ulman A, Schildkraut JS, Penner TL. Incorporation of phenoxy groups in self-assembled monolayers of trichlorosilane derivatives – effects on film thickness, wettability, and molecular-orientation. J Am Chem Soc 1988;110(18):6136–44.
[33] Ederth T, Tamada K, Claesson PM, Valiokas R, Colorado R, Graupe M, et al. Force measurements between semifluorinated thiolate self-assembled monolayers: long-range hydrophobic interactions and surface charge. J Colloid Interface Sci 2001;235(2):391–7.
[34] Wenzel RN. Resistance of solid surfaces to wetting by water. J Ind Eng Chem 1936;28(8):988–94.
[35] Deng K, Collins RJ, Mehregany M, Sukenik CN. Performance impact of monolayer coating of polysilicon micromotors. J Electrochem Soc 1995;142(4): 1278–85.
[36] Stewart S, Ahmed R. Rolling contact fatigue of surface coatings—a review. Wear 2002;253(11–12):1132–44.
[37] Sjöström H, Wikström V. Diamond-like carbon coatings in rolling contacts. Proc IMechE Part J: J Eng. Tribol. 2001;215(6):545–61.